The importance of thermal electron heating in Titan's ionosphere: Comparison with Cassini T34 flyby

Y. J. Ma,[1] C. T. Russell,[1] A. F. Nagy,[2] G. Toth,[2] M. K. Dougherty,[3] A. Wellbrock,[4] A. J. Coates,[4] P. Garnier,[5,6] J.-E. Wahlund,[5] T. E. Cravens,[7] M. S. Richard,[7] and F. J. Crary[8]

Received 16 March 2011; revised 10 June 2011; accepted 24 July 2011; published 15 October 2011.

[1] We use a new magnetohydrodynamic (MHD) model to study the effects of thermal-electron heating in Titan's ionosphere. This model improves the previously used multispecies MHD model by solving both the electron and ion pressure equations instead of a single plasma pressure equation. This improvement enables a more accurate evaluation of ion and electron temperatures inside Titan's ionosphere. The model is first applied to an idealized case, and the results are compared in detail with those of the single-pressure MHD model to illustrate the effects of the improvement. Simulation results show that the dayside ionosphere thermal pressure is larger than the upstream pressure during normal conditions, when Titan is located in the dusk region; thus Saturn's magnetic field is shielded by the highly conducting ionosphere, similar to the interaction of Venus during solar maximum conditions. This model is also applied to a special flyby of Titan, the T34 flyby, which occurred near the dusk region. It is shown that better agreement with the magnetometer data can be achieved using the two-fluid MHD model with the inclusion of the effects of thermal electron heating. The model results clearly demonstrate the importance of thermal-electron heating in Titan's ionosphere.

Citation: Ma, Y. J., et al. (2011), The importance of thermal electron heating in Titan's ionosphere: Comparison with Cassini T34 flyby, *J. Geophys. Res.*, *116*, A10213, doi:10.1029/2011JA016657.

1. Introduction

[2] The plasma interaction around Titan is similar to the solar wind interaction with nonmagnetized planets, such as Venus and Mars. A unique interaction structure near Venus, as observed by Pioneer Venus Orbiter (PVO), is the formation of the ionopause when solar wind dynamic pressure is less than the peak of the ionospheric thermal pressure [*Luhmann et al.*, 1980]. The interplanetary magnetic field is shielded by the highly conducting ionosphere under such conditions. In order to understand the Cassini magnetic field observations during low-altitude passes, it is important to determine the relative strength of the ram-side ionospheric thermal pressure and the upstream plasma pressure.

[3] When Titan orbits Saturn, the flowing magnetospheric plasma can interact with the dayside ionosphere, nightside ionosphere or somewhere in between. To make the interaction more complicated, the plasma environment around Titan is also highly variable; Titan could be located in Saturn's plasma sheet, lobe or magntosheath region [*Rymer et al.*, 2009]. In addition, the magnetic field is also highly perturbed near Titan's orbit most of the time [*Simon et al.*, 2010].

[4] The magnetic pressure and ionospheric pressure profiles measured by the Cassini spacecraft were discussed in detail for the first Titan flyby by *Wahlund et al.* [2005]. It was found that the magnetic pressure of the magnetosphere and the electron thermal pressure of the ionosphere were largely of the same order of magnitude during the TA flyby. They also found that the "ionopause" was not sharply defined, but rather smeared over an extended region on both the inbound and outbound trajectories, since the Cassini spacecraft mainly passed through the wake region of Titan during the flyby. A recent study by *Edberg et al.* [2010] showed that statistically, the peak of the thermal pressure plus magnetic pressure is less than the dynamic pressure of the magnetospheric plasma; in other words, the magnetic field should be able to penetrate inside the ionosphere in most cases. However, the majority of those flybys occurred away from the ram direction.

[1] Institute of Geophysics and Planetary Physics, University of California, Los Angeles, California, USA.
[2] Department of Atmospheric, Oceanic, and Space Sciences, University of Michigan, Ann Arbor, Michigan, USA.
[3] Space and Atmospheric Physics Group, Blackett Laboratory, Imperial College London, London, UK.
[4] Mullard Space Science Laboratory, University College London, Dorking, UK.
[5] Swedish Institute of Space Physics, Uppsala, Sweden.
[6] Institut de Recherche en Astrophysique et Planétologie, UMR 5277 Université de Toulouse, Université Paul Sabatier–OMP, CNRS, Toulouse, France.
[7] Department of Physics and Astronomy, University of Kansas, Lawrence, Kansas, USA.
[8] Southwest Research Institute, San Antonio, Texas, USA.

0148-0227/11/2011JA016657

[5] Although a single-fluid MHD model can predict the density and magnetic field in fairly good agreement with the observations [*Ma et al.*, 2006], it does not do a good job in reproducing the electron temperature inside the ionosphere [*Ulusen et al.*, 2010]. The single-fluid MHD model only solves for the plasma pressure (= ion pressure + electron pressure), so it cannot provide separate values for ion and electron temperatures. A simple assumption that the ion temperature equals electron temperature is usually used when the ion or electron temperature is needed to evaluate dissociative recombination rates and to calculate energy transfer between ions and neutrals. In fact, electron temperature is usually different from the ion temperature. For example, the ion temperature in the Saturnian magnetosphere near Titan's orbit is normally higher than the electron temperature; while in Titan's ionosphere, the electron temperature is dominant over the ion temperature. At low altitudes at Titan, because of the tight coupling between ions and neutrals due to frequent ion-neutral collisions, the ion temperature is nearly the same as the neutral temperature. The coupling between electrons and neutrals is not as tight especially in the sunlit ionosphere as discussed by *Galand et al.* [2006]. The temperature of thermal electrons is usually higher than neutrals due to heating through collisions with the superthermal electrons, which consist of photo and secondary as well as magnetospheric electrons [*Gan et al.*, 1992, 1993; *Roboz and Nagy*, 1994; *Richard et al.*, 2011]. The electron temperature (assuming it to be the same as the ion temperature) as predicted by the model is quite low in comparison with the Langmuir probe (LP) observations in Titan's ionosphere, as can be seen in the work of *Ma et al.* [2006, Figure 6]. Even though the thermal electron heating can be added in the total pressure equation, the energy is lost quickly through collisions between ions and neutrals when assuming the electron temperature to be infinitely tightly coupled to the ion temperature. Thus, the only way to solve the problem is to separate the temperatures of electrons and ions in the model, solving two pressure equations for electrons and ions, respectively. The same problem remains even in the hybrid simulation, since the electron temperature is either assumed to be to zero [*Kallio et al.*, 2004] or assumed to be adiabatic [*Simon et al.*, 2006; *Modolo et al.*, 2005], which means that both energy source and loss of electrons are neglected.

[6] This is the first attempt to address this problem in a global interaction model. In section 2, the two-fluid MHD model used in the paper will be discussed in detail. Section 3 compares simulation results of an ideal case using both a two-fluid MHD model and a single-fluid MHD model, and discusses the importance of the two-pressure equations in Titan's ionosphere. Section 4 applies the model to Cassini T34 flyby and compares the model results with plasma observations. A brief summary is given in section 5.

2. Two-Fluid MHD Model

[7] The seven-species single-fluid MHD model has been used to study the first two Titan flybys of Cassini [*Ma et al.*, 2006]. In this study, the model is improved by solving two separate pressure equations for electrons and ions, so that both electron temperature and ion temperature can be self-consistently calculated. In this model, electrons and ions are treated as two separate fluids, and their density, velocity and temperatures are all calculated self-consistently. The complete set of equations of the two fluid MHD model includes the following:

Continuity equation for seven ion species

$$\frac{\partial \rho_i}{\partial t} + \nabla \cdot (\rho_i \mathbf{u}) = S_i - L_i,$$
$$S_i = m_i n_{i'} \left(\nu_{\mathrm{ph},i'} + \nu_{\mathrm{imp},i'} + \sum_{s=\mathrm{ions}} k_{si'} n_s \right), \quad (1)$$
$$L_i = m_i n_i \left(\alpha_{R,i} n_e + \sum_{n=\mathrm{neutrals}} k_{in} n_n \right),$$

Momentum equation for ions (assuming all the ions have the same velocity)

$$\frac{\partial(\rho \mathbf{u})}{\partial t} + \nabla \cdot \left(\rho \mathbf{u}\mathbf{u} + (p + p_e)\mathbf{I} + \frac{B^2}{2\mu_0}\mathbf{I} - \frac{1}{\mu_0}\mathbf{B}\mathbf{B} \right)$$
$$= \rho \mathbf{G} - \sum_{i=\mathrm{ions}} \rho_i \sum_{n=\mathrm{neutrals}} \nu_{in}(\mathbf{u} - \mathbf{u}_n) + \sum_{i=\mathrm{ions}} (S_i \mathbf{u}_n - L_i \mathbf{u}), \quad (2)$$

where $\rho = \sum_{i=\mathrm{ions}} \rho_i$, Ion pressure equation

$$\frac{\partial Pi}{\partial t} + (\mathbf{u} \cdot \nabla) Pi + \gamma Pi (\nabla \cdot \mathbf{u}) = \sum_{i=\mathrm{ions}} \sum_{n=\mathrm{neutrals}} \frac{\rho_i \nu_{in}}{m_i + mn}$$
$$\cdot \left[2k(T_n - T_i) + (\gamma - 1) m_n (\mathbf{u}_n - \mathbf{u})^2 \right]$$
$$+ \sum_{i=\mathrm{ions}} v_{ie} n_i n_e (T_e - T_i) 2k + \frac{(\gamma - 1)}{2} \sum_{i=\mathrm{ions}} S_i (\mathbf{u}_n - \mathbf{u})^2$$
$$+ \sum_{i=\mathrm{ions}} \left(\frac{S_i T_n - L_i T_i}{m_i} k \right), \quad (3)$$

Electron density can be calculated using

$$n_e = \sum_{i=\mathrm{ions}} \frac{\rho_i}{m_i}. \quad (4)$$

Electron velocity is defined as

$$\mathbf{u}e = \mathbf{u} + \mathbf{u}_H = \mathbf{u} - \frac{\mathbf{J}}{ne}, \quad (5)$$

where $\mathbf{u}_H$ is the Hall velocity, defined as $\mathbf{J}/ne$ to indicate the velocity differences between ions and electrons.

[8] The electron pressure equation is

$$\frac{\partial P_e}{\partial t} + (\mathbf{u_e} \cdot \nabla) P_e + \gamma P_e (\nabla \cdot \mathbf{u_e})$$
$$= \sum_{i=\mathrm{ions}} v_{ie} n_i n_e (T_i - T_e) 2k + (\gamma - 1) \sum_{i=\mathrm{ions}} n_{i'} v_{ph,i'} E_0$$
$$+ \sum_{n=\mathrm{neutrals}} v_{ne} n_n n_e (T_n - T_e) 2k - \sum_{i=\mathrm{ions}} n_i \alpha_{R,i} n_e T_e k + \frac{(\gamma - 1)}{\sigma_0} j^2. \quad (6)$$

The magnetic conduction equation with a resistivity term is

$$\frac{\partial \mathbf{B}}{\partial t} + \nabla \cdot (\mathbf{u}\mathbf{B} - \mathbf{B}\mathbf{u}) = \nabla \times \left(\frac{1}{\sigma_0 \mu_0} \nabla \times \mathbf{B} \right). \quad (7)$$

Note that in the induction equation, the Hall term is neglected. We will discuss the effects of the Hall term in detail in a following paper. The magnetic field is frozen in with the ions where resistivity is not important. The following definitions are used in equations (1)–(7):

$[\ ]_{i,s}$ ion species index;
$[\ ]_e$ electron;
$[\ ]_{n,i'}$ neutral species index, where i' refers to the parent neutral of the ith ion species;
ρ_i mass densities of seven different pseudo-ion species as listed in previous Titan papers [*Ma et al.*, 2006];
S_i, L_i ion mass production and loss rates, calculated according to the chemical reactions in which these ions are involved;
m_i, n_i mass and number density of corresponding neutrals;
$\nu_{\mathrm{ph},i'}$, $\nu_{\mathrm{imp},i'}$ corresponding photoionization rates and impact ionization rates;
$\alpha_{R,i}$ recombination rate;
$k_{s,i'}$, k_{in} charge exchange reaction rates;
$\mathbf{u}$, $\mathbf{u}_e$, $\mathbf{u}_n$ velocity of the ions, electrons, and neutrals, respectively;
$\mathbf{J}$, j electric current vector and strength;
P_i, P_e ion and electron thermal pressure, respectively;
T_i, T_e ion and electron temperature, respectively;
γ ratio of specific heats, taken to be 5/3;
μ_0 permeability of free space, which is $4\pi \times 10^{-7}$ H/m;
σ_0 electrical conductivity of the plasma; the conductivity is calculated using the same method described by *Ma et al.* [2006];
T_n neutral temperature, taken to be 150 K, to be consistent with the Cassini INMS observations [*Waite et al.*, 2005];
ν_{in} momentum transfer collision frequency between ions and neutrals, calculated using the same method as described by *Schunk and Nagy* [2009];
ν_{ie} momentum transfer collision frequencies between ions and electrons, calculated using the same method described by *Schunk and Nagy* [2009];
ν_{ne} momentum transfer collision frequencies between neutrals and electrons, calculated based on the temperature-dependent collision rates with neutrals N_2 and CH_4 [*Gan et al.*, 1992; *Gan and Cravens*, 1992; *Richard et al.*, 2011];
E_0 average energy imparted to the bulk thermal electron population by newly produced photoelectrons.

[9] The mass density of each ion species is calculated using the continuity equation (1). The changes in the ion mass density depend on the convection $\nabla\cdot(\rho\mathbf{u})$ term, source (S_i), and loss (L_i) terms. The convection term is important in regions above the ionopause, while in the lower ionosphere, the density is mainly determined by the production and loss rates calculated based on chemical reactions.

[10] The momentum equation (2) describes the variation of the plasma moments. The terms on the left-hand side are the same as in an ideal MHD model. The two terms on the right-hand side are the loss due to ion-neutral collisions and changes due to chemical reactions. The relative importance of different forces varies not only with altitude but also the relative angle to the flow direction and solar radiation direction, as discussed in detail by *Ulusen et al.* [2010].

[11] Equation (3) describes the change in ion pressure, including the heating effect due to ion-electron Coulomb collisions and the cooling effect caused by ion-neutral collisions. Similarly, electron cooling due to electron-ion collisions and electron–neutral collisions are included in the electron pressure equation (equation (6)). Thermal electron heating is also included as the second term on the right-hand side of equation (6). Here, the thermal electron heating is assumed to be proportional to the photoionization rates. We assume that the thermal electron heating rate due to Coulomb collisions with photoelectrons is a characteristic energy (E_0 = 0.6 eV) multiplied by the photoionization rate. This estimate was based on a detailed electron energy efficiency calculation from an ionospheric energetics model of Titan that includes photoelectron transport and collisions with neutrals and thermal electrons [*Richard et al.*, 2011]. Also note that heat conduction is neglected in the model as is the neutral wind ($\mathbf{u}_n$ is set to zero).

[12] The above set of equations is solved using the Michigan BATS-R-U.S. code [*Powell et al.*, 1999; *Tóth et al.*, 2011]. Similar to our previous simulations of Titan, the inner boundary is set at 725 km altitude. The boundary conditions are described in detail by *Ma et al.* [2009]. We use a spherical grid structure with the finest radial resolution of about 16 km close to the inner boundary and a total of about 2 million grid cells. The simulations are completed using a NASA super computer. Each run requires about 1000 processor hours.

3. Two-Fluid MHD Model Versus Single-Fluid MHD Model

[13] We first apply the above model to an idealized case of Titan. The upstream plasma condition was set as follows:

$$n_L^+ = 0.1/\mathrm{cc},\ n_M^+ = 0.1/\mathrm{cc},\ T_e = 200\,\mathrm{eV};\ T_i = 1500\,\mathrm{eV};$$
$$U = [120,\ 0,\ 0]\,\mathrm{km/s};\ B = [0, 0, -5]nT.$$

The coordinate system used in the paper follows the commonly used Titan Interaction coordinate system (TIIS) [*Backes et al.*, 2005]. With the above set of parameters, Titan faces a subsonic (with sonic Mach number M_S = 0.63) and submagnetosonic (magnetosonic Mach number M_{MS} = 0.57) but super-Alfvenic (Alfvenic Mach number M_A = 1.3) magnetospheric plasma flow. Titan is assumed to be located in the 18 Saturnian Local Time (SLT), meaning that the upstream co-rotational plasma would interact directly with the dayside ionosphere of Titan, as in the solar wind–planetary interactions. In order to show the importance of the electron pressure equation, we also applied the single fluid MHD model using the same set of parameters, except the upstream electron and ion temperatures are set to be the same 850 eV value.

[14] Figure 1 shows plasma flow and magnetic field results in both the equatorial (*XY*) and polar (*XZ*) plane for the two-fluid MHD model. The color shows plasma flow speed (Figures 1a and 1b) and magnetic field strength (Figures 1c and 1d), and white arrows show projections of flow directions (Figures 1a and 1b) and magnetic field directions

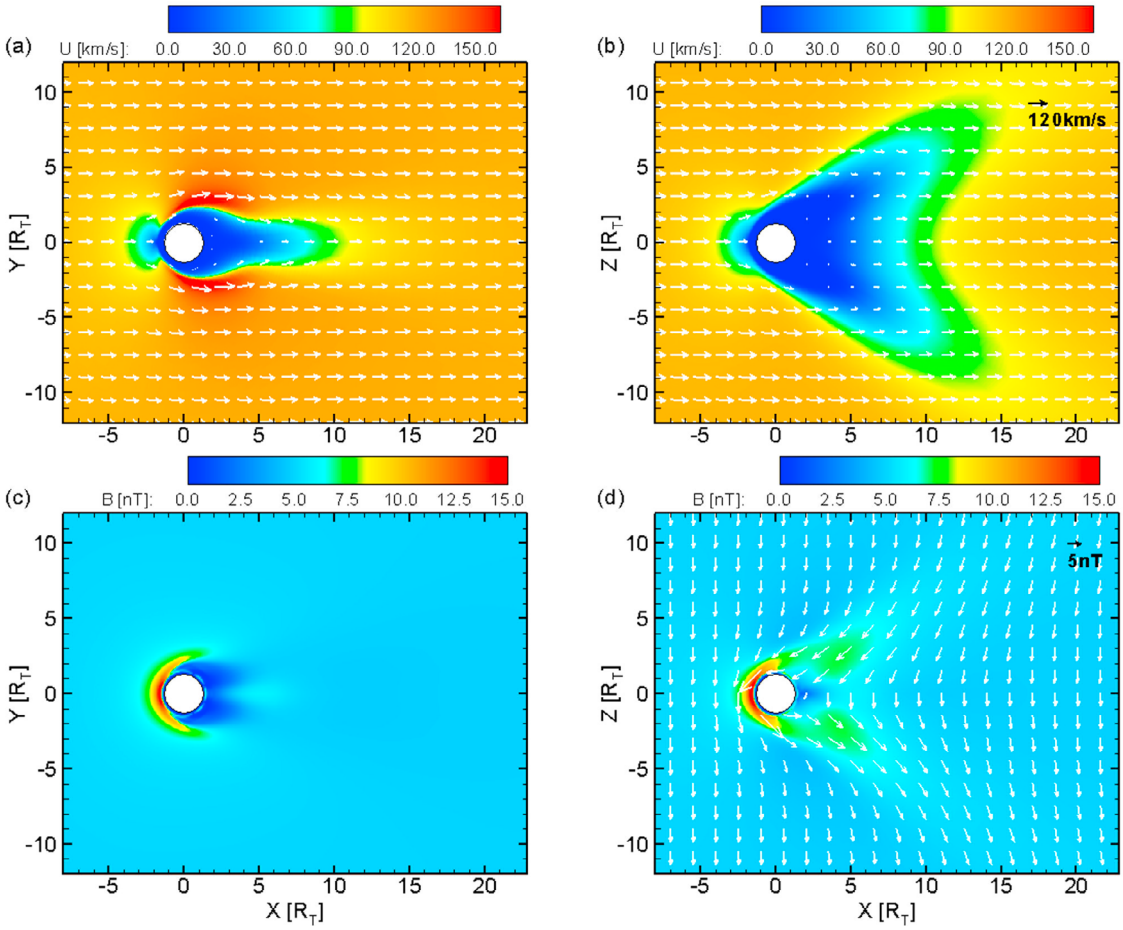

Figure 1. Contour plots of plasma flow speed and magnetic field strength in the equatorial (*XY*) and polar (*XZ*) planes. The white arrows show projections of (a, b) flow directions and (c, d) magnetic field directions in the corresponding plane for the two-fluid magnetohydrodynamic (MHD) model.

(Figures 1c and 1d). The magnetic field vector does not show in the *XY* plane, because the magnetic field is mainly in the *Z* direction. The global interaction structure is similar to that of the MHD model [*Ma et al.*, 2004] including slowing down of the plasma flow in the region close to the moon; piling up and draping of the magnetic field around the obstacle; the forming of a pair of Alfven wings along the magnetic field direction. Because magnetic field is mainly in the *Z* direction, the plasma flow pattern in the *XY* and *XZ* plane are significantly different. The acceleration in the flank region of Titan in the equatorial plane (*XY*) is caused by magnetic tension force. This demonstrates that solving separate pressure equations for ions and electrons in the model, as long the upstream plasma total pressure is set to be the same, will result in similar large-scale results. However, the two models predict significantly different magnetic fields in the ionosphere of Titan, which will be discussed in detail later. It is also worth noting that the result of single fluid MHD is symmetric in the *XY* plane, while hybrid simulation produces asymmetric interaction pattern in this plane due to ion pickup process [*Brecht et al.*, 2000].

[15] Figure 2 shows contour plots of electron number density and plasma pressure ($P_e + P_i$) in the equatorial (*XY*) and polar (*XZ*) plane with the two-fluid MHD model. In comparison, Figure 3 plots results of the single-fluid MHD model in the same format. There are some differences in the plasma flank and wake regions for the electron number density. The plasma extends further in the tail region for two-fluid MHD. Also, the plasma pressure is much higher in the ionosphere for the two-fluid MHD case, mainly contributed by the electron pressure, in comparison with the single-fluid MHD case. The transterminator fluxes for heavy ion species (mass ≥ 28) are 1.0×10^{24} ions/s, corresponding to 52.5 g/s mass transport for both cases. The total escape rate is 3.3×10^{24} ions/s for the single-fluid MHD case and increases about 12% when using two fluid MHD model. The transterminator fluxes are similar to the values estimated by *Cui et al.* [2010], but total escape fluxes of the MHD models are smaller than their estimate ($\sim 1.7 \times 10^{25}$). Even though the ion pressure of the two-fluid model is similar to that predicted by the regular MHD model, the electron temperature (pressure) in the ionosphere is high because of thermal electron heating and the loose coupling between the electrons and ions/neutrals. As a result, the thermal pressure in the ionosphere is high enough to stand off the upstream plasma flow and stop the magnetic field from penetrating the ionosphere.

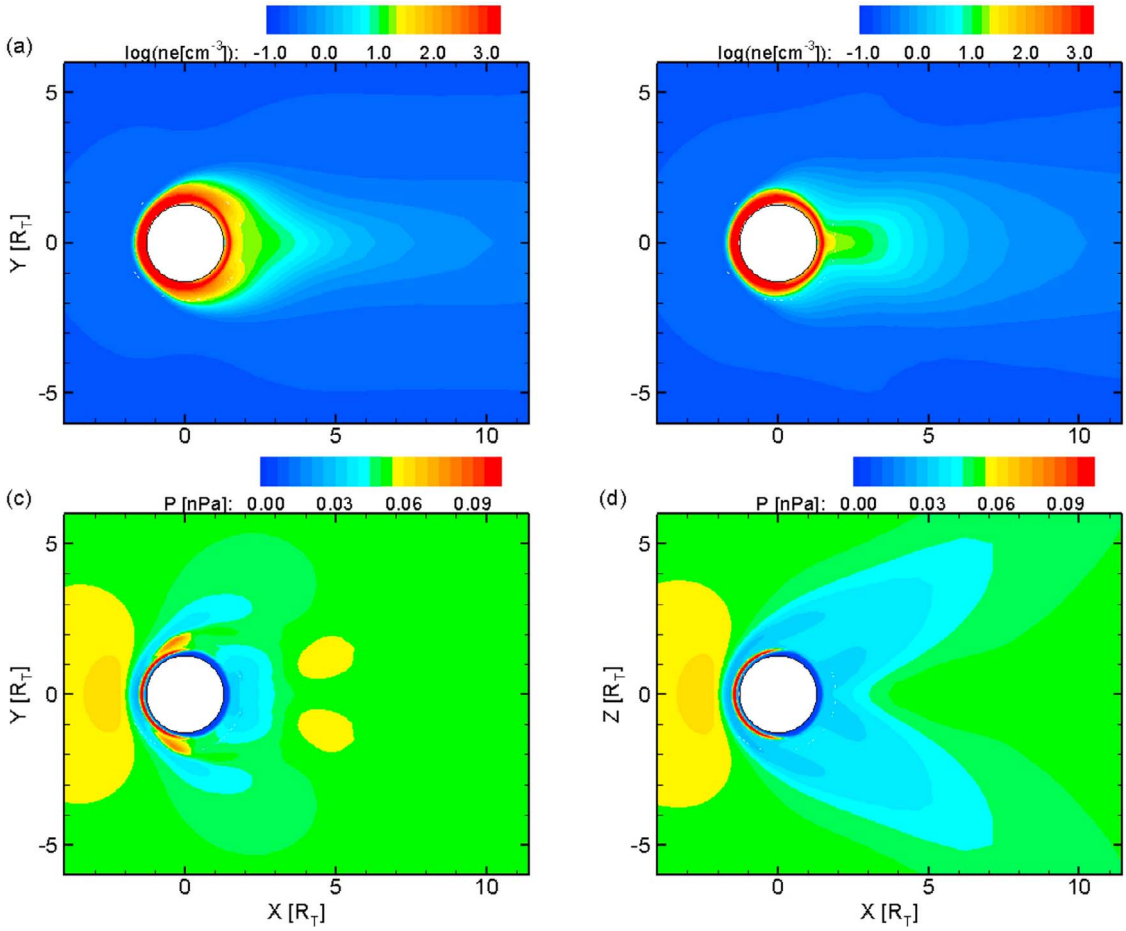

Figure 2. Contour plots of electron number density and plasma pressure ($P_e + P_i$) in the equatorial (*XY*) and polar (*XZ*) planes for the two-fluid MHD model.

[16] This can also be clearly seen in Figure 4, which plots the pressure profiles versus altitude along the ram direction for both the single-fluid MHD (Figure 4a) and two-fluid MHD (Figure 4b) models. For each case, the magnetic pressure P_B ($B^2/2\mu_0$), dynamic pressure P_D (ρu^2), thermal pressure of the plasma P_T, electron thermal pressure P_e, ion thermal pressure P_i and total pressure P_{TOTAL} (the sum of magnetic pressure P_B, dynamic pressure P_D, and thermal pressure P_T) are plotted. In the single-fluid MHD model, only the plasma thermal pressure is calculated, and P_e and P_i are just assumed to be the same ($P_T/2$). According to the parameters used in the case, the thermal pressure, dynamic pressure and magnetic pressure of the unperturbed plasma are 0.054 nPa, 0.036 nPa, and 0.01 nPa, respectively. In both cases, the thermal pressure is dominant in the unperturbed plasma flow. Both the dynamic pressure and thermal pressure are converted into magnetic pressure as the plasma moves inward along the ram direction (the plasma flow slows down and cools as a result of mass loading). Significant slow down of the plasma starts from about $4R_T$ upstream, while the cooling of the plasma is important below 3000 km altitude. Because the coupling between ions and neutrals is tight, the resulting ion temperature is close to neutrals in the deep ionosphere for both cases. The main differences between the two models are in the electron and magnetic pressures in the ionosphere. Since the coupling between electrons and neutrals is weak; the electrons have a higher temperature than the ions/neutrals due to thermal electron heating. The peak of the thermal pressure in the ionosphere is around 0.04 nPa in the case of the single-fluid model, while it is roughly 3 times that value for the two-fluid model, which is contributed mainly by the electron pressure. The upstream total pressure is slightly smaller than the peak of the thermal pressure in the two-fluid MHD case. As a result, the magnetic field penetration is stopped by the conducting ionosphere, at 1000 km in this case. In contrast, the magnetic field piles up all the way to 900 km and only drops to zero due to magnetic diffusion at very low altitudes, in the case of the single-fluid MHD model. Using empirical estimations, *Cravens et al.* [2010] also found that the structure of the magnetic field is dominated by magnetic diffusion at altitudes below ~1000 km, consistent with the analysis of *Ulusen et al.* [2010] based on the T5 flyby.

4. Observations and Model Comparisons of the T34 Flyby

[17] In this section, we apply the two-fluid MHD model to the T34 flyby, described in some detail by *Simon et al.* [2008]. During this flyby, Cassini passed Titan at 0111 UT

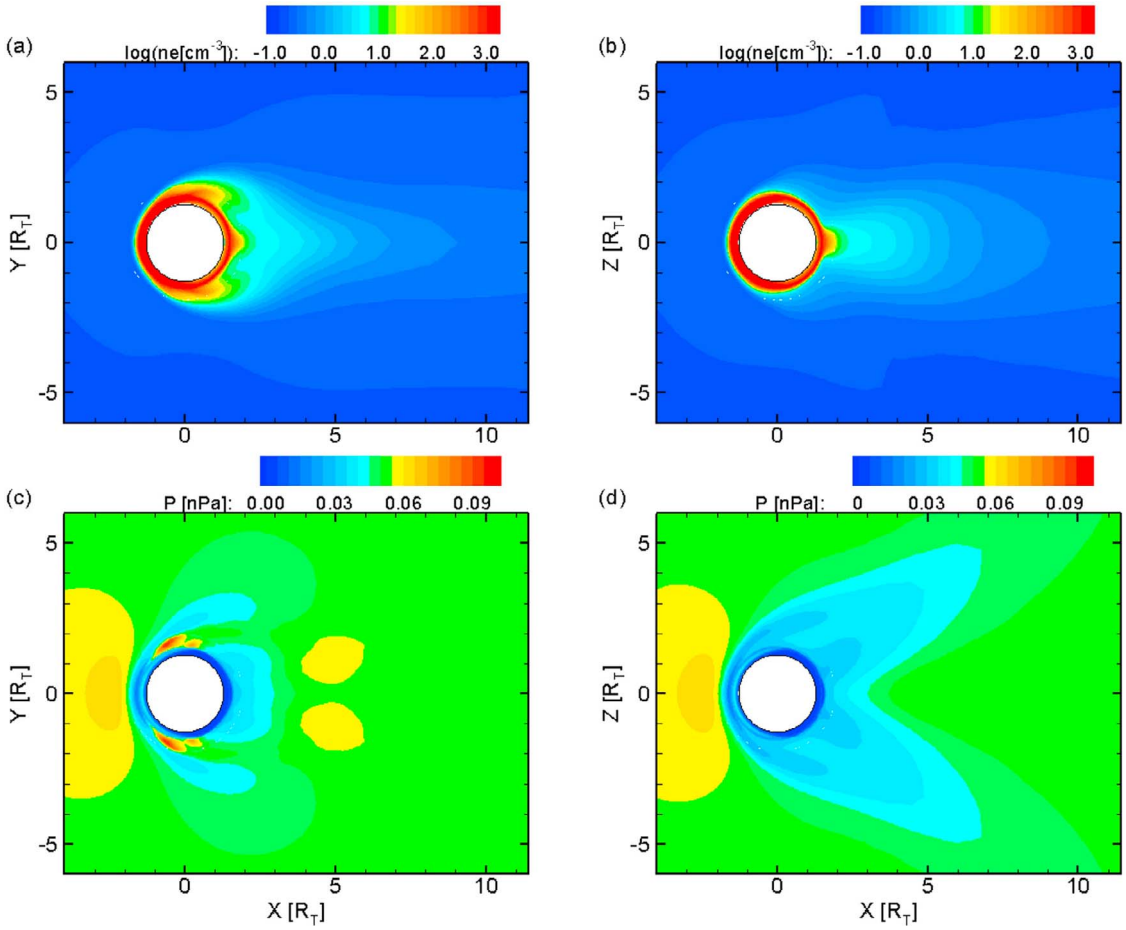

Figure 3. Contour plots of electron number density and plasma pressure ($P_e + P_i$) in the equatorial (*XY*) and polar (*XZ*) planes for the single-fluid MHD model.

on 19 July 2007, with the closest approach at 1332 km altitude from Titan's surface. As shown in Figure 5, the spacecraft trajectory lies almost exactly in the equatorial plane of Titan. The blue squares show the spacecraft location at 10 min intervals. Titan is located at the dusk sector at 18.8 SLT during the flyby, indicating that the upstream co-rotational plasma would interact mostly with the dayside ionosphere of Titan, similar to the solar wind–planetary interaction. This is the only flyby to date that Cassini passed through the low ionosphere (<1500 km altitude) of Titan from the upstream side of the equatorial plane. The magnetic field vector and field strength observed by the magnetometer [*Dougherty et al.*, 2004] are overplotted with the trajectory. A clear draping pattern can be seen in the magnetic field vectors in Figure 5 (left). The magnetic field pileup is also clearly shown in the plot as the vector length increases in the intermediate region, also indicated by the color denoting the magnitude of the field strength.

[18] We use the two-fluid MHD model to simulate this flyby. The direction of the Sun during the flyby is set to (−0.958, 0.21, −0.20). The upstream density is set to 0.76 amu/cc, with 0.06/cc H^+ and 0.05/cc M^+, where H^+ and M^+ denote light ion species and median ion species based on Cassini Plasma Spectrometer (CAPS) [*Young et al.*, 2004] observations, respectively. The plasma magnetic field is set to $B = [-1.0, 2.3, -2.1]$ nT, based on mean background magnetic field observations. The magnetic field magnitude is therefore 3.27 nT. This field is similar to the values used by *Simon et al.* [2008], but the upstream plasma density is smaller than that used by *Simon et al.* [2008], in which a Voyager-like plasma density was used. The plasma is assumed to be flowing along the co-rotation direction with a speed of 150 km/s. Titan faces a submagnetosonic (magnetosonic Mach number: $M_{MS} = 0.9$), yet super-Alfvenic (Alfvenic Mach number: $M_A = 1.8$) magnetospheric plasma flow.

[19] Figure 6 shows data and model comparisons of plasma density, velocity and temperature for the single-fluid (Figure 6a) and two-fluid (Figure 6b) models during the T34 flyby. As can be seen in Figure 6 (top), both models reproduce well the plasma density along the trajectory. The predicted peak of the electron number density is somewhat larger than observed by the Langmuir Probe (LP). The sharp drop of the electron density across the ionopause when moving to higher altitudes is well reproduced by the models for both inbound and outbound passes. Both models predict that across the ionopause, the plasma flow speed drops more sharply during the inbound pass than outbound, as shown in Figure 6 (middle). However, the two models predict significantly different temperature profiles for electrons along the

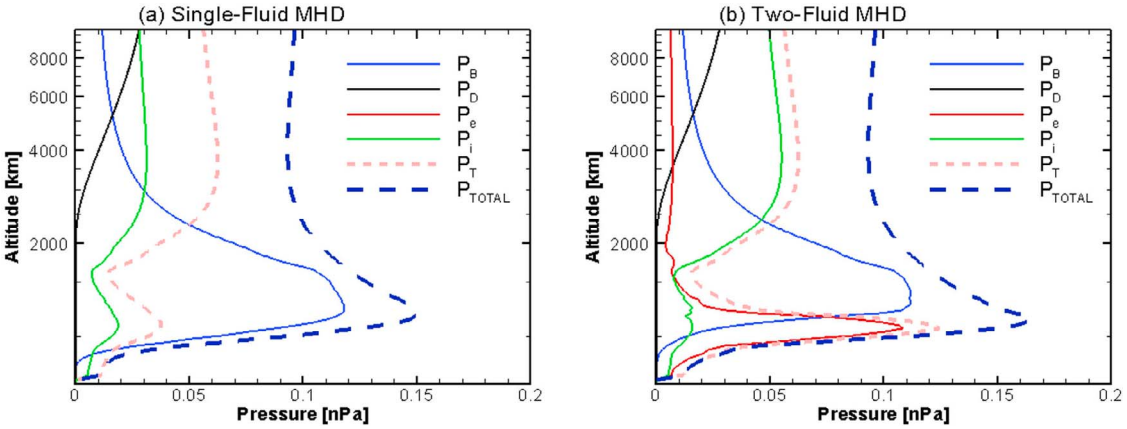

Figure 4. Pressure profiles along the ram direction for the (a) single-fluid and (b) two-fluid models. In each case, the magnetic pressure $P_B = B^2/2\mu_0$, dynamic pressure $P_D = \rho u^2$, electron thermal pressure $P_e = n_e k T_e$, ion thermal pressure $P_i = n_i k T_i$, plasma thermal pressure $P_T = P_e + P_i$, and total pressure $P_{\mathrm{TOTAL}} = P_B + P_D + P_T$ are plotted.

trajectory as shown in Figure 6 (bottom). The single-fluid MHD model predicts that inside the ionosphere, both electron and ion temperatures are the same as the neutral temperature. The ion temperature of the two-fluid model is also nearly the same as the neutral temperature in the ionosphere, but the electron temperature is much higher than that of the ions due to the reasons that stated before. At the closest approach, the electron temperature is about 800 K according to LP observations, while the estimations from the single fluid model and the two-fluid model are 150 K and 2300 K, respectively. In comparison, the ion temperatures from those two models are 150 K and 160 K, respectively. Apparently, the two-fluid model is able to produces higher electron temperature than that of the neutrals and ions in the lower ionosphere that better matched the observations. However, the calculated electron temperature is somewhat higher than LP observations in the ionosphere. This could be due to (1) overestimation of the characteristic energy due to thermal electron heating or (2) underestimation of electron-neutral cooling rates.

[20] Data and model comparisons of the magnetic field during the T34 flyby for the single-fluid and two-fluid models are illustrated in Figure 7 with the measured (black lines) and the simulated (red lines) signatures along the

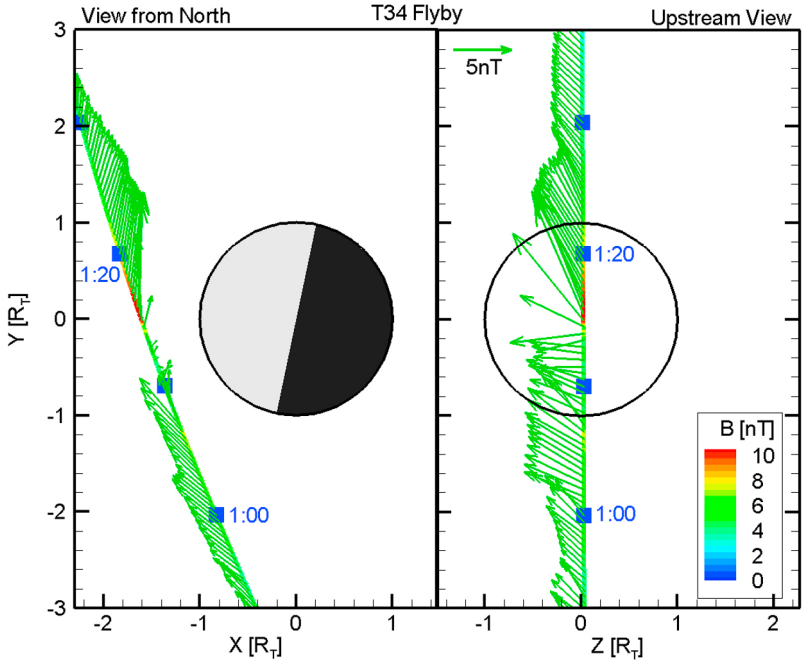

Figure 5. Trajectory and magnetometer observations of the T34 flyby projected in the equatorial (*XY*) and flow terminator (*YZ*) planes. The color shows the strength of the magnetic field. The blue squares show the spacecraft location at 10 min intervals.

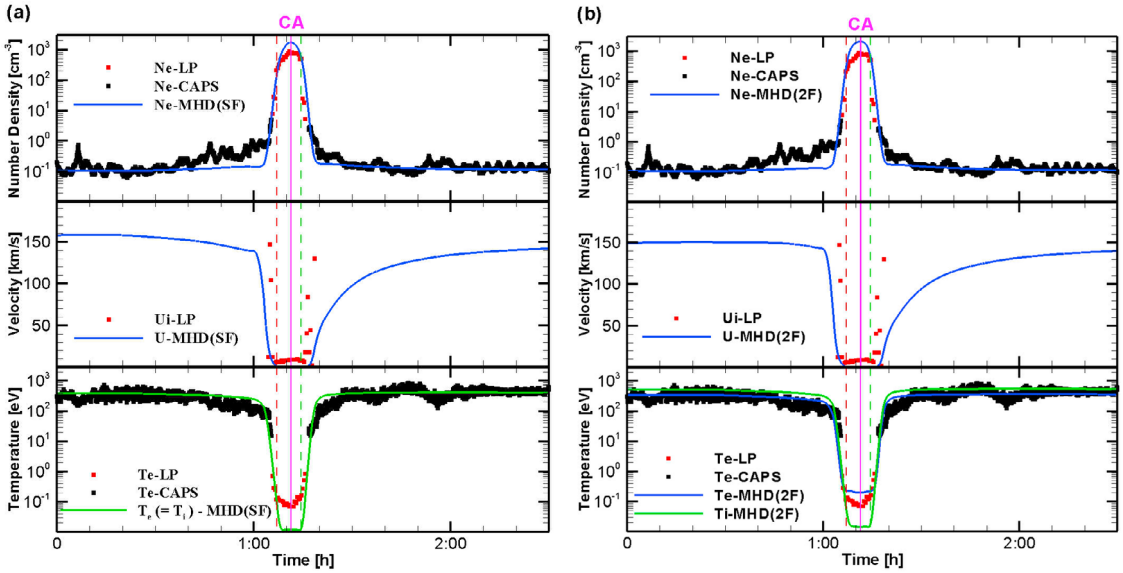

Figure 6. Data and model comparisons of plasma electron number density, velocity, and temperature for (a) single-fluid and (b) two-fluid models for the T34 flyby. The red symbols show Langmuir probe (LP) observations, the black symbols are Cassini Plasma Spectrometer (CAPS) observations, and blue and green lines are MHD model results.

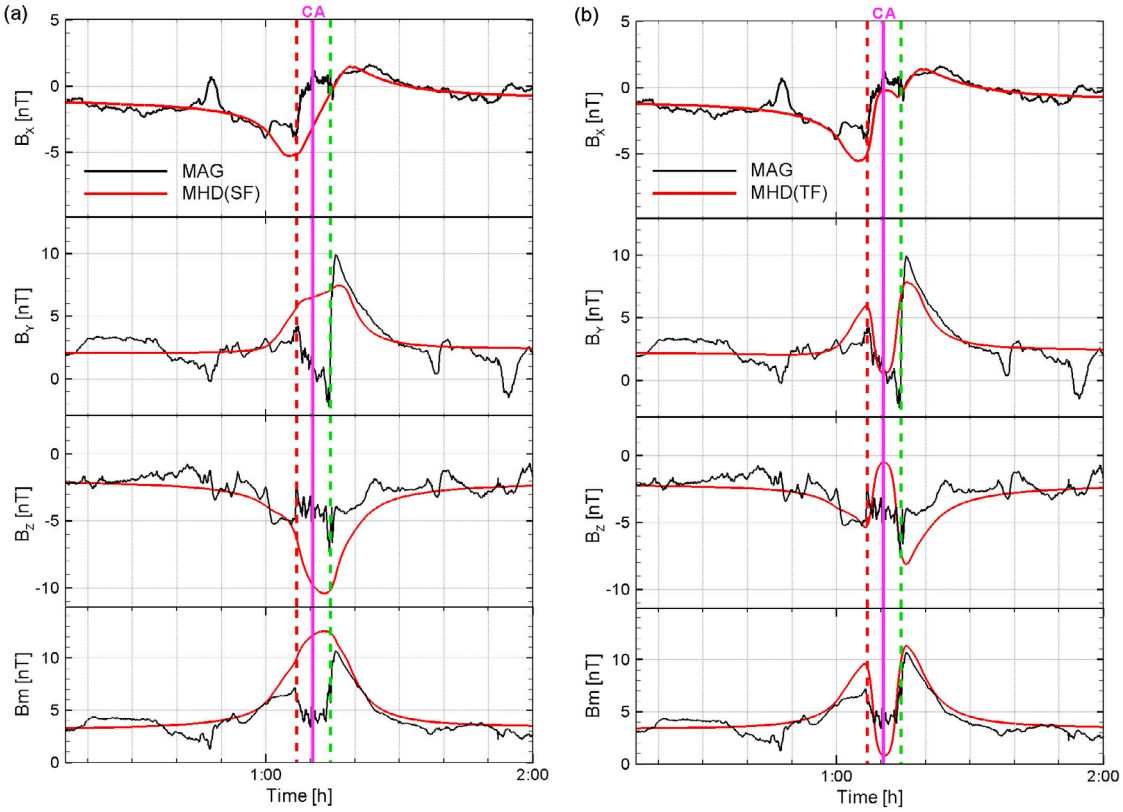

Figure 7. Data and model comparisons of the magnetic field during the T34 flyby for the (a) single-fluid and (b) two-fluid MHD models. The black lines show observed magnetic fields, while the red lines are from the MHD model results.

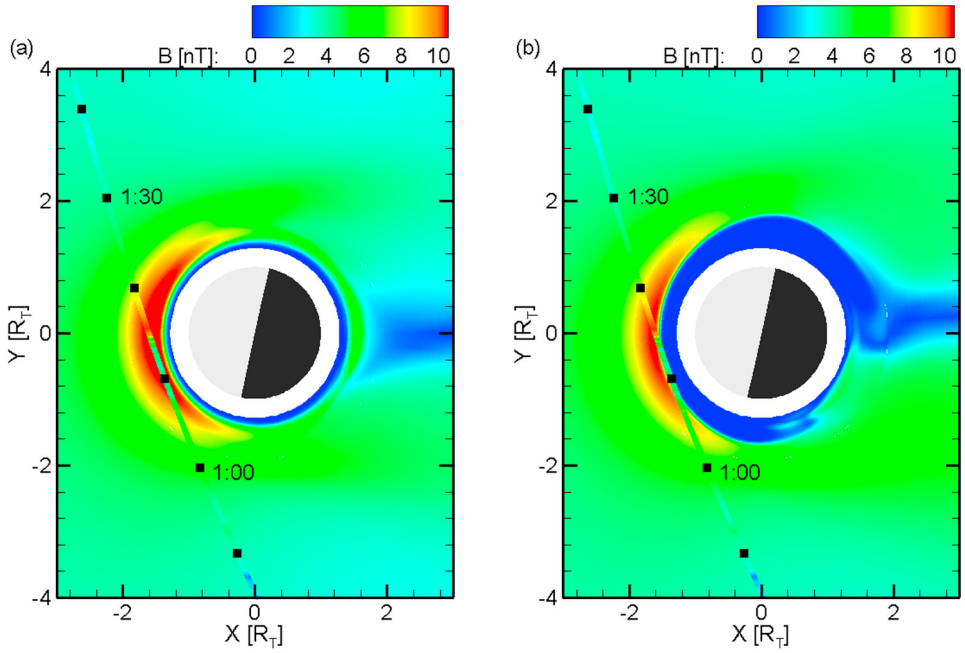

Figure 8. Contour plots of magnetic field strength in the *XY* plane for the (a) single-fluid and (b) two-fluid models. The T34 trajectory shown by the black squares (10 min interval) and colored with magnetometer measurements is overplotted.

trajectory. The main features of the observed magnetic field have been discussed, in detail, by *Simon et al.* [2008]. The single-fluid MHD model predicts a B_X dip, a strong enhancement of B_Y and B_Z and B near closest approach. These signatures agree well with observations especially outside of the ionopause as indicated by the two dashed lines marked at 0106 UT and 0115 UT, corresponding to 1650 km and 1515 km during inbound and outbound passes. Also the calculated B_X, B_Y, and B are similar to that predicted by the hybrid model of *Simon et al.* [2008]. Both the hybrid and single-fluid MHD models predict that the magnetic field reaches all the way to the lower ionosphere, in contrast to the observations.

[21] The sharp changes of the magnetic field across the ionopause are only reproduced with the two-fluid MHD model as shown in Figure 7a. This is because the two-fluid model is able to reproduce the high electron temperature in the ionosphere, and the thermal pressure in the ionosphere is crucial to obtaining the correct magnetic field behavior in the region. Both observation and model show that at least occasionally, Titan's ionosphere can stop the magnetic field from penetrating inside. It should also be noted that the value inside the ionosphere for modeled B_z and B are somewhat different from the values observed. The differences are likely caused by the fossil field resulting from interactions with previous plasma conditions [*Bertucci et al.*, 2008], in which the upstream plasma pressure is high enough to cause the penetration of the magnetic field. Because of the slow convection of the plasma in the ionosphere, the fossil magnetic field can last for hours [*Ma et al.*, 2009].

[22] The differences of the two model results are also clearly shown in Figure 8. Both models predict the pileup of the magnetic field in the upstream region. The magnetic field penetrates deeper into the ionosphere in the single-fluid model, in comparison with the two-fluid model. The sharp decrease of the observed magnetic field strength matches better with the two-fluid model results. Because the upstream plasma flow is assumed to be along the co-rotation flow direction, the pileup region is symmetric about the flow direction. In contrast, the observations seem to indicate that the flow is tilted toward the negative Z direction. The asymmetry is unlikely to be caused by ion pickup process or associated finite gyroradius effects since hybrid simulation by *Simon et al.* [2008] also failed to reproduce the different peak values of magnetic field strength during inbound and outbound passes.

5. Summary

[23] We have used our new two-fluid multispecies MHD model to study the effects of thermal electron heating in Titan's ionosphere. This model presents an improvement over the previously used multispecies single-fluid MHD model by solving both the electron and ion pressure equations instead of a single plasma pressure equation. This improvement enables a more accurate evaluation of ion and electron temperatures inside Titan's ionosphere. We show the importance of the improvement by applying the two-fluid MHD model to an ideal case and comparing the results with that of the single-fluid MHD model. Simulation results show that the dayside ionosphere thermal pressure is larger than the upstream pressure when Titan is located in the dusk region; thus the magnetic field is shielded by the highly conducting ionosphere in this situation, similar to the interaction of Venus during solar maximum conditions. The model is also applied to the T34 flyby of Cassini, which occurred near the dusk region. Model results show that it is critical to include thermal electron heating in order to

reproduce the key features that are observed in the ionosphere by the magnetometer and the Langmuir probe.

[24] The two-fluid MHD model is an important improvement over the single-pressure MHD model. It is able to self-consistently calculate separate electron and ion temperatures, and can help us to better understand the behavior of the magnetic field inside the ionosphere. Please note that the Hall Effect as well as neutral wind coupling is neglected in the model presented in this paper. Their effects could be important in some regions as suggested by *Ulusen et al.* [2010] and will be discussed in future studies.

[25] **Acknowledgments.** Philippa Browning thanks Edward Sittler Jr. and another reviewer for their assistance in evaluating this paper.

References

Backes, H., et al. (2005), Titan's magnetic field signature during the first Cassini encounter, *Science*, *308*, 992–995, doi:10.1126/science.1109763.

Bertucci, C., et al. (2008), The magnetic memory of Titan's ionized atmosphere, *Science*, *321*, 1475–1478, doi:10.1126/science.1159780.

Brecht, S. H., J. G. Luhmann, and D. J. Larson (2000), Simulation of the Saturnian magnetospheric interaction with Titan, *J. Geophys. Res.*, *105*, 13,119–13,130, doi:10.1029/1999JA900490.

Cravens, T. E., et al. (2010), Dynamical and magnetic field time constants for Titan's ionosphere: Empirical estimates and comparisons with Venus, *J. Geophys. Res.*, *115*, A08319, doi:10.1029/2009JA015050.

Cui, J., M. Galand, R. V. Yelle, J.-E. Wahlund, K. Ågren, J. H. Waite Jr., and M. K. Dougherty (2010), Ion transport in Titan's upper atmosphere, *J. Geophys. Res.*, *115*, A06314, doi:10.1029/2009JA014563.

Dougherty, M. K., et al. (2004), The Cassini magnetic field investigation, *Space Sci. Rev.*, *114*, 331–383, doi:10.1007/s11214-004-1432-2.

Edberg, N. J. T., J.-E. Wahlund, K. Ågren, M. W. Morooka, R. Modolo, C. Bertucci, and M. K. Dougherty (2010), Electron density and temperature measurements in the cold plasma environment of Titan: Implications for atmospheric escape, *Geophys. Res. Lett.*, *37*, L20105, doi:10.1029/2010GL044544.

Galand, M., R. V. Yelle, A. J. Coates, H. Backes, and J.-E. Wahlund (2006), Electron temperature of Titan's sunlit ionosphere, *Geophys. Res. Lett.*, *33*, L21101, doi:10.1029/2006GL027488.

Gan, L., and T. E. Cravens (1992), Electron impact cross sections and cooling rates for methane, *Planet. Space Sci.*, *40*, 1535–1544, doi:10.1016/0032-0633(92)90050-X.

Gan, L., C. N. Keller, and T. E. Cravens (1992), Electrons in the ionosphere of Titan, *J. Geophys. Res.*, *97*, 12,137–12,151, doi:10.1029/92JA00300.

Gan, L., T. E. Cravens, and C. N. Keller (1993), A time-dependent model of suprathermal electrons at Titan, in *Plasma Environments of Non-magnetic Planets*, vol. 4, edited by T. I. Gombosi, pp. 171–176, Elsevier, New York.

Kallio, E., I. Sillanpää, and P. Janhunen (2004), Titan in subsonic and supersonic flow, *Geophys. Res. Lett.*, *31*, L15703, doi:10.1029/2004GL020344.

Luhmann, J. G., R. C. Elphic, C. T. Russell, J. D. Mihalov, and J. H. Wolfe (1980), Observations of large scale steady magnetic fields in the dayside Venus ionosphere, *Geophys. Res. Lett.*, *7*, 917–920, doi:10.1029/GL007i011p00917.

Ma, Y., A. F. Nagy, T. E. Cravens, I. V. Sokolov, J. Clark, and K. C. Hansen (2004), 3-D global MHD model prediction for the first close flyby of Titan by Cassini, *Geophys. Res. Lett.*, *31*, L22803, doi:10.1029/2004GL021215.

Ma, Y., A. F. Nagy, T. Cravens, I. V. Sokolov, K. C. Hansen, J. Wahlund, F. Crary, A. Coates, and M. Dougherty (2006), Comparisons between MHD model calculations and observations of Cassini flybys of Titan, *J. Geophys. Res.*, *111*, A05207, doi:10.1029/2005JA011481.

Ma, Y. J., et al. (2009), Time-dependent global MHD simulations of Cassini T32 flyby: From magnetosphere to magnetosheath, *J. Geophys. Res.*, *114*, A03204, doi:10.1029/2008JA013676.

Modolo, R., G. M. Chanteur, E. Dubinin, and A. P. Matthews (2005), Influence of the solar EUV flux on the Martian plasma environment, *Ann. Geophys.*, *23*, 433–444, doi:10.5194/angeo-23-433-2005.

Powell, K. G., P. L. Roe, T. J. Linde, T. I. Gombosi, and D. L. De Zeeuw (1999), A solution-adaptive upwind scheme for ideal magnetohydrodynamics, *J. Comput. Phys.*, *154*, 284–309, doi:10.1006/jcph.1999.6299.

Richard, M. S., T. E. Cravens, I. P. Robertson, J. H. Waite, J.-E. Wahlund, F. J. Crary, and A. J. Coates (2011), Energetics of Titan's ionosphere: Model comparisons with Cassini data, *J. Geophys. Res.*, *116*, A09310, doi:10.1029/2011JA016603.

Roboz, A., and A. F. Nagy (1994), The energetics of Titan's ionosphere, *J. Geophys. Res.*, *99*, 2087–2093, doi:10.1029/93JA02286.

Rymer, A. M., H. T. Smith, A. Wellbrock, A. J. Coates, and D. T. Young (2009), Discrete classification and electron energy spectra of Titan's varied magnetospheric environment, *Geophys. Res. Lett.*, *36*, L15109, doi:10.1029/2009GL039427.

Schunk, R. W., and A. F. Nagy (2009), *Ionospheres*, Cambridge Univ. Press, New York, doi:10.1017/CBO9780511635342.

Simon, S., A. Bößwetter, T. Bagdonat, U. Motschmann, and K.-H. Glassmeier (2006), Plasma environment of Titan: A 3-D hybrid simulation study, *Ann. Geophys.*, *24*, 1113–1135, doi:10.5194/angeo-24-1113-2006.

Simon, S., U. Motschmann, G. Kleindienst, K. Glassmeier, C. Bertucci, and M. K. Dougherty (2008), Titan's magnetic field signature during the Cassini T34 flyby: Comparison between hybrid simulations and MAG data, *Geophys. Res. Lett.*, *35*, L04107, doi:10.1029/2007GL033056.

Simon, S., A. Wennmacher, F. M. Neubauer, C. L. Bertucci, H. Kriegel, J. Saur, C. T. Russell, and M. K. Dougherty (2010), Titan's highly dynamic magnetic environment: A systematic survey of Cassini magnetometer observations from flybys TA-T62, *Planet. Space Sci.*, *58*, 1230–1251, doi:10.1016/j.pss.2010.04.021.

Tóth, G., et al. (2011), Adaptive numerical algorithms in space weather modeling, *J. Comput. Phys.*, in press, doi:10.1016/j.jcp.2011.02.006.

Ulusen, D., J. G. Luhmann, Y.-J. Ma, S. Ledvina, T. E. Cravens, K. Mandt, J. H. Waite, and J.-E. Wahlund (2010), Investigation of the force balance in the Titan ionosphere: Cassini T5 flyby model/data comparisons, *Icarus*, *210*, 867–880, doi:10.1016/j.icarus.2010.07.004.

Wahlund, J.-E., et al. (2005), Cassini measurements of cold plasma in the ionosphere of Titan, *Science*, *308*, 986–989, doi:10.1126/science.1109807.

Waite, J. H., et al. (2005), Ion neutral mass spectrometer results from the first flyby of Titan, *Science*, *308*, 982–986, doi:10.1126/science.1110652.

Young, D. T., et al. (2004), The Cassini plasma spectrometer, *Space Sci. Rev.*, *114*, 1–112, doi:10.1007/s11214-004-1406-4.

A. J. Coates and A. Wellbrock, Mullard Space Science Laboratory, University College London, Dorking RH5 6NT, UK.

F. J. Crary, IRAP, CNRS, 9 Ave. Colonel Roche, BP 44346, F-31028 Toulouse CEDEX 4, France.

T. E. Cravens and M. S. Richard, Department of Physics and Astronomy, University of Kansas, 1251 Wescoe Hall Dr., Malott Hall, Lawrence, KS 66045, USA.

M. K. Dougherty, Space and Atmospheric Physics Group, Blackett Laboratory, Imperial College London, Exhibition Road, London SW7 2AZ, UK.

P. Garnier and J.-E. Wahlund, Swedish Institute of Space Physics, Box 537, Uppsala SE-75121, Sweden.

Y. J. Ma and C. T. Russell, Institute of Geophysics and Planetary Physics, University of California, 6877 Slichter Hall, Los Angeles, CA 90095, USA. (yingjuan@igpp.ucla.edu)

G. Toth and A. F. Nagy, Department of Atmospheric, Oceanic, and Space Sciences, University of Michigan, 2455 Hayward, Ann Arbor, MI 48109-2143, USA.